

# Nature of spin glass order in physical dimensions

Bharadwaj Vedula,<sup>1</sup> M. A. Moore,<sup>2</sup> and Auditya Sharma<sup>1</sup>

<sup>1</sup>*Department of Physics, Indian Institute of Science Education and Research, Bhopal, Madhya Pradesh 462066, India*

<sup>2</sup>*Department of Physics and Astronomy, University of Manchester, Manchester M13 9PL, United Kingdom*

(Dated: October 28, 2024)

We have studied the diluted Heisenberg spin glass model in a 3-component random field for the commonly-used one-dimensional long-range model where the probability that two spins separated by a distance  $r$  interact with one another falls as  $1/r^{2\sigma}$ , for two values of  $\sigma$ , 0.75 and 0.85. No de Almeida-Thouless line is expected at these  $\sigma$  values. The spin glass correlation length  $\xi_{\text{SG}}$  varies with the random field as expected from the Imry-Ma argument and the droplet scaling picture of spin glasses. However, when  $\xi_{\text{SG}}$  becomes comparable to the system size  $L$ , there are departures which we attribute to the features deriving from the TNT picture of spin glasses. For the case  $\sigma = 0.85$  these features go away for system sizes with  $L > L^*$ , where  $L^*$  is large ( $\approx 4000 - 8000$  lattice spacings). In the case of  $\sigma = 0.75$  we have been unable to study large enough systems to determine its value of  $L^*$ . We sketch a renormalization group scenario to explain how these features could arise. On this scenario finite size effects on the droplet scaling picture in low-dimensional spin glasses produce TNT features and some aspects of Parisi's replica symmetry breaking theory of the Sherrington-Kirkpatrick model.

## I. INTRODUCTION

The nature of the ordered state of spin glasses has been controversial for nearly four decades. Newman and Stein have suggested that there are at least four possibilities for the ordered state [1] which are not disallowed by rigorous arguments: the broken replica symmetry (RSB) picture of Parisi, [2–6], the chaotic pairs state of Newman and Stein [7], the TNT picture of Palassini and Young [8] and Houdayer, Krzakala and Martin [9, 10] and the droplet scaling picture [11–13]. These different types of ordered states are distinguished by the free energy cost of droplet excitations whose size is comparable to the size of the system  $L$ , and the fractal dimension  $d_s$  of the droplet surface. For the RSB picture and the TNT picture there are excitations of size  $L$  which contain  $L^d$  spins in  $d$  dimensions with an associated free energy cost of  $O(1)$ . In the chaotic pairs and droplet scaling picture the free energy cost of such excitations increases as  $L^{\theta'}$ , with  $\theta' > 0$ . For the RSB and chaotic pairs pictures, the fractal dimension of the droplet surface has  $d_s = d$ , so that the droplet surface is space filling. In the droplet and TNT scaling pictures  $d_s < d$  but on the TNT picture the large droplets of order of the system size  $L$  have a fractal surface dimension  $d_s = d$  [9] while on the droplet picture they retain the same surface fractal dimension as that of smaller droplets,  $d_s$ . A recent numerical study of spin glass excitations whose energies are of  $O(1)$  in two and three dimensions can be found in Ref. [14].

The application of a magnetic field helps to differentiate the four pictures. In the presence of a field there can still be a phase transition in the RSB picture. This is the de Almeida-Thouless (AT) transition [15]. At the AT transition the paramagnetic high-temperature replica symmetric state becomes a state with broken replica symmetry. There is a similar transition in the chaotic pairs picture. However, in the TNT picture and the droplet scaling picture there is no phase transition in a field. Re-

cently we have carried out simulations of the AT transitions and found evidence that the AT line goes away below six dimensions [16]. Then if so, below six dimensions the ordered state must be either that of the TNT picture or that of droplet scaling.

In this paper we present evidence that in low dimensions, such as  $d = 3$ , the ordered state is that according to droplet scaling, and that evidence for the TNT picture arises from finite size effects. We find that droplets whose size  $\mathcal{L}$  is less than the linear size  $L$  of the system have excitation energies which behave as expected on the droplet picture, increasing as  $\mathcal{L}^{\theta'}$ . Finite size effects invariably complicate numerical studies but in the case of spin glasses they produce features which have also confused the search for the correct order parameter. Experiments are not usually affected by finite size effects, but for them there is the related issue of making the size of regions which are fully equilibrated large enough [17]. The droplet scaling picture predicts according to Fisher and Huse [13] that droplets at site  $i$  which contain  $i$  and which are of scale  $\mathcal{L}$  (which means that they contain more than  $\mathcal{L}^d$  spins but less than  $(2\mathcal{L})^d$  spins), have a free energy ( $F$ ) distribution  $\rho(F, \mathcal{L})$ , which in the limit of large  $\mathcal{L}$ , has the scaling form

$$\rho(F, \mathcal{L}) = \frac{1}{\mathcal{L}^{\theta'}} \tilde{\rho}\left(\frac{F}{\mathcal{L}^{\theta'}}\right). \quad (1)$$

An exponent  $\theta$  is usually defined via the variance of the free energy when the boundary conditions are changed from  $\uparrow\uparrow$  to  $\uparrow\downarrow$  or from periodic to anti-periodic boundary conditions across a system of linear dimension  $L$ ;  $(F_{\uparrow\uparrow} - F_{\uparrow\downarrow})^2 \sim L^{2\theta}$ . In the droplet picture the exponent  $\theta'$  is equal to the domain wall exponent  $\theta$ . In the RSB picture  $\theta = d/6$  but  $\theta' = 0$  [18, 19]. Thus in the RSB picture there are system-wide droplets whose free energy is only of  $O(1)$ . These droplets are space filling, that is the fractal dimension of their interfaces has  $d_s = d$ .

Eq. (1) only applies when the droplet scale  $\mathcal{L}$  is smaller

than the linear dimension  $L$  of the system (or the size of its fully equilibrated region). When  $\mathcal{L}$  is comparable to  $L$  then finite size effects come into play which produce the effects captured by the TNT picture. In Sec. III we explain using a renormalization group (RG) argument how these finite size effects which arise when the system's correlation length  $\xi_{\text{SG}}$  is of the order of system size  $L$  can produce some of the RSB features found in the Parisi approach to the Sherrington-Kirkpatrick (SK) [20] model. We also explain that if the system size  $L$  is greater than some large length  $L^*$  then these RSB features should disappear. This reflects what is seen in our Monte Carlo simulations at  $\sigma = 0.85$ . In [21] it was suggested that  $L^*$  becomes infinite as  $d \rightarrow 6$  because the excitations of free energy  $O(1)$  become the excitations of  $O(1)$  of the RSB picture. When  $L < L^*$  our RG argument suggests that the Parisi overlap function  $P(q)$  at  $q = 0$ , (which is expected to behave as  $T/L^{\theta'}$  on the droplet picture) should be an  $L$  independent constant, just as on the RSB picture [17, 22]. In previous studies it has not been possible to simulate low dimensional systems which have linear dimensions  $L$  large enough so that the TNT features can be seen to be finite size effects, but in this paper we have managed to study systems which do have  $L > L^*$ . They support the droplet picture as being the correct description of spin glasses in three dimensions, with TNT effects and apparent RSB effects arising from finite size effects.

It is only possible to directly study large droplets for two-dimensional Ising spin glasses by numerical methods [23–25]. There exist no fast algorithms which will make studies in higher dimensions very convincing. In two dimensions there are departures from Eq. (1) due to finite size effects which can be described by conventional finite size scaling arguments, viz that the standard deviation of the energy of droplets  $\Delta E(\mathcal{L})$ , varies as

$$\Delta E(\mathcal{L}) \sim \mathcal{L}^{\theta'} (1 + B\mathcal{L}^{-\omega}), \quad (2)$$

where  $\omega$  is the correction to scaling exponent associated with the zero-temperature fixed point and  $B$  gives the magnitude of this correction to scaling. In two dimensions the length scale below which these finite size modifications of Eq. (1) are noticeable seems to be of order roughly 60 lattice spacings [24, 25]. Thus only for droplets larger than 60 lattice spacings across is the simple  $\mathcal{L}^{\theta'}$  visible. For domain walls, in two dimensions, asymptopia sets in at much smaller sizes, presumably due to having a smaller correction to scaling coefficient  $B$ . In early work, using sizes only up to  $L = 12$ , Bray and Moore [26] found the stiffness exponent  $\theta$  for the size dependence of domain wall excitations to be  $-0.294 \pm 0.009$ . This was close to more recent results [23] using much better methods, which enabled study of sizes from  $L = 8$  to 10,000, with the result that  $\theta = -0.2793 \pm 0.0003$ . In the metastate study of Hartmann and Young [27] in two dimensions they found that the large  $L$  behavior was reached by  $L = 8$  as it was domain walls and not droplets which determined the approach to asymptopia in their work. This suggests that it

would be worthwhile to extend their work to three dimensions. In two dimensions the metastate behavior which they found was that predicted by the droplet picture.

The finite size effects which we believe explain TNT effects (and their similarity to RSB effects) and their disappearance above a system size  $L^*$  is of different origin to that in Eq. (2) (see Sec. III). They arise because when  $\xi_{\text{SG}}$  is of order  $L$ , the behavior of the system is largely determined by the  $k = 0$  mode of the underlying field theory  $q_{\alpha\beta}$ , as in the finite size studies of Brézin and Zinn-Justin [28]. It is this which produces a parallel with the SK model. It has been known for a long time that even in the one-dimensional Ising spin glass model with short-range interactions that many of the features usually associated with the Parisi solution of the SK model can be found when the correlation length approaches the length of the system [29].

TNT effects are visible in quantities such as the Parisi overlap function  $P(q)$  which involves the  $k = 0$  mode of  $q_{\alpha\beta}$ . There are, however, situations where the important excitations are *not* of the size of the system. An example of these arises in the phenomena of temperature chaos [13, 30, 31]. If the temperature is changed from a value  $T_1$  to  $T_2$ , (where both are smaller than the transition temperature  $T_c$ ) then above a length scale  $\mathcal{L}_c$  the spin orientations are completely modified, where

$$\mathcal{L}_c(T_1, T_2) \sim \frac{1}{(T_2 - T_1)^{1/\zeta}}. \quad (3)$$

The exponent  $\zeta = d_s/2 - \theta'$  (at least on the droplet picture). This formula is obtained by equating the free energy cost of flipping all the spins in a region of size  $\mathcal{L}_c$ , which scales as  $\mathcal{L}_c^{\theta'}$ , to the free energy which can be gained from variations of the droplet surface entropy, which is of  $O((T_2 - T_1)\mathcal{L}_c^{d_s/2})$ . Values of  $\mathcal{L}_c$  in simulations of three dimensional Ising spin glasses are usually of only a few lattice spacings (and hence much smaller than the linear dimensions  $L$  of the system), and hence one would expect good agreement with droplet model scaling ideas. This is indeed the case. According to [32, 33], for the Ising spin glass in three dimensions  $d_s \approx 2.60(2)$ , while Boettcher [34] claims  $\theta' \approx 0.24(1)$ . The temperature chaos exponent  $\zeta$  has been estimated [35] to be 1.04, which is therefore in good agreement with droplet model expectation based on the value  $\zeta = d_s/2 - \theta' = 1.06$ . Note that if the values of  $d_s$  and  $\theta'$  predicted by replica symmetry breaking, viz  $d_s = d = 3$  and  $\theta' = 0$ , then the value of  $\zeta$  would be 1.5, which is much larger than its observed value. In the case of the SK model the choices  $d_s = d$  and  $\theta' = 0$  are consistent with the results on chaos obtained by Parisi and Rizzo [36]. Because of the success of the droplet scaling picture in explaining the chaos length scale when it is small, we shall assume that the droplets of free energy of  $O(1)$  in the TNT picture arise only when the droplets are of the system size  $L$ . This was the original proposal of Houdayer and Martin [9]. These droplets on the scale of the system size  $L$  are supposed

to be “sponge-like” and have  $d_s = d$ , just like those in the RSB scenario.

In the next section we describe the one-dimensional Heisenberg spin glass proxy model and our Monte Carlo simulations of it. In Sec. III we outline the renormalization group scenario which is consistent with the existence of TNT behavior as a finite size effect and its apparent disappearance for system sizes larger than  $L^*$ . Finally in Sec. IV we review our results and discuss what remains to be done.

## II. THE MODEL AND SIMULATIONS

We study the same one-dimensional proxy model which we recently used to determine the behavior of the AT line as  $d \rightarrow 6$  [16]. Its Hamiltonian is that of the classical Heisenberg spin glass in a 3-component random field

$$\mathcal{H} = - \sum_{\langle i,j \rangle} J_{ij} \mathbf{S}_i \cdot \mathbf{S}_j - \sum_i \mathbf{h}_i \cdot \mathbf{S}_i, \quad (4)$$

where  $\mathbf{S}_i$  is a classical spin on the  $i^{\text{th}}$  lattice site ( $i = 1, 2, \dots, N$ ), and is a unit vector of  $m = 3$  components. The  $N$  lattice sites are arranged around a circle. Each pair of spins  $(i, j)$  are separated by a distance  $r_{ij}$  and the geometric distance between a pair of spins  $(i, j)$  is given by [37]

$$r_{ij} = \frac{N}{\pi} \sin \left( \frac{\pi}{N} |i - j| \right), \quad (5)$$

which is just the length of the chord connecting the  $i^{\text{th}}$  and  $j^{\text{th}}$  spins. The interactions  $J_{ij}$  are independent random variables such that the probability of having a non-zero interaction between a pair of spins  $(i, j)$  falls with the distance  $r_{ij}$  between the spins as a power law:

$$p_{ij} = \frac{r_{ij}^{-2\sigma}}{\sum_{j \neq i} r_{ij}^{-2\sigma}}. \quad (6)$$

If the spins  $i$  and  $j$  are linked the magnitude of the interaction between them is drawn from a Gaussian distribution of zero mean and whose standard deviation is unity, i.e:  $[J_{ij}]_{\text{av}} = 0$  and  $[J_{ij}^2]_{\text{av}} = J^2 = 1$ . To generate the set of interaction pairs [38, 39]  $(i, j)$  with the desired probability we pick a site  $i$  randomly and uniformly and then choose a second site  $j$  with probability  $p_{ij}$ . If the spins at  $i$  and  $j$  are already connected we repeat this process until we find a pair of sites  $(i, j)$  which have not been connected. Once we find such a pair of spins, we connect them with a bond whose strength  $J_{ij}$  is a Gaussian random variable with the above attributes. We repeat this process exactly  $N_b$  times to generate  $N_b$  pairs of interacting spins.

The mean number of non-zero bonds from a site is chosen to be  $\tilde{z}$  (the co-ordination number). The total number of bonds among all the spins on the lattice is

$N_b = N\tilde{z}/2$ . When  $\tilde{z} = 6$  this feature is that also of the 3D simple cubic lattice model and this value for  $\tilde{z}$  was used for both the  $\sigma$  values studied. For  $\sigma = 0$  and  $\tilde{z} = N - 1$ , the model becomes the infinite-range Sherrington-Kirkpatrick (SK) model [20], where the zero-field transition temperature is  $T_c = \sqrt{\tilde{z}}/m$ . The Cartesian components  $h_i^\mu$  of the on-site external field are independent random variables drawn from a Gaussian distribution of zero mean with each component having variance  $h_r^2$ .

Models similar to this have already been studied [39, 40]. Even though it involves spins of  $m (=3)$  components, its AT transition (when it exists) is in the universality class of the Ising ( $m = 1$ ) model [41]. Despite the additional degrees of freedom of the spins compared to those of the Ising model, the Heisenberg model is easier to simulate than the Ising model as the vector spins provide a means to go around barriers rather than over them as in the Ising case, allowing larger systems to be simulated [42]. We ourselves have extensively studied the XY ( $m = 2$ ) version of it [43], when we concentrated mainly on cases with  $\sigma = 0.75$  and  $\sigma = 0.85$ . Since writing that paper we have discovered that the Heisenberg case ( $m = 3$ ) runs slightly faster, and so in this paper we have studied these same values of  $\sigma$  but for the Heisenberg model. The results relating to TNT effects have turned out to be strikingly similar to those found for the XY model [43], even though the exponent which describes the behavior of the correlation length differs (see Table II). The mapping from  $\sigma$  to a finite dimensionality  $d_{\text{eff}}$  is complicated when  $\sigma > 2/3$ , but, in Ref. [44], it was argued that the Ising version of our system with  $\sigma = 0.896$  corresponded to  $d_{\text{eff}} = 3$ , while  $\sigma = 0.790$  corresponded to a value of  $d_{\text{eff}} = 4$ . When  $\sigma = 2/3$ ,  $d_{\text{eff}} = 6$ .

The simulation methods employed in this study follow the approach outlined in our previous work [16, 41, 43]. We use a combination of overrelaxation and heatbath sweeps, following a 10:1 ratio, where ten overrelaxation sweeps are performed for every heatbath sweep [42, 45]. Overrelaxation sweeps, also known as microcanonical sweeps, allow the system to explore microstates at constant energy, while heatbath sweeps enable proper equilibration by sampling states with different energies according to the Boltzmann distribution. The parameters for the simulations, including equilibration times and the number of disorder samples, are listed in Table I.

To verify that the system has reached equilibrium, we apply a test that leverages the Gaussian nature of the interactions and the external magnetic field [46]. The equilibrium condition is validated by the relation

$$U = \frac{\tilde{z}J^2}{2T} (q_l - q_s) + \frac{h_r^2}{T} (q - |\mathbf{S}|^2), \quad (7)$$

where  $U = \frac{1}{N} [\langle \mathcal{H} \rangle]_{\text{av}}$  is the average energy per spin,  $q = \frac{1}{N} \sum_i [\langle \mathbf{S}_i \rangle \cdot \langle \mathbf{S}_i \rangle]_{\text{av}}$  is the Edwards-Anderson order parameter,  $q_l = \frac{1}{N_b} \sum_{\langle i,j \rangle} [\epsilon_{ij} \langle \mathbf{S}_i \cdot \mathbf{S}_j \rangle^2]_{\text{av}}$  is the “link

overlap”, and  $q_s = \frac{1}{N_b} \sum_{\langle i,j \rangle} \left[ \epsilon_{ij} \langle (\mathbf{S}_i \cdot \mathbf{S}_j)^2 \rangle \right]_{\text{av}}$  is the “spin overlap”, where  $N_b = N\tilde{z}/2$ , and  $\epsilon_{ij} = 1$  if the  $i^{\text{th}}$  and  $j^{\text{th}}$  spins are interacting and is zero otherwise. As the system evolves, the left-hand side (LHS) of this equation starts small while the right-hand side (RHS) is large, and the two approach each other from opposite directions as equilibrium is reached. We calculate both sides of the equation over increasing numbers of Monte Carlo sweeps (MCSs), with each value doubling the previous one. The system is considered to be in equilibrium once the averaged values of Eq. (7) match within error bars for at least two consecutive points. Upon reaching equilibrium, we transition to the measurement phase to investigate the system’s properties, with relevant simulation parameters shown in Table I.

We focus in this paper on determining and understanding the spin glass correlation length  $\xi_{\text{SG}}$ . The wavevector-dependent susceptibility is defined via [39]

$$\chi_{\text{SG}}(k) = \frac{1}{N} \sum_{i,j} \frac{1}{m} \sum_{\mu,\nu} \left[ (\chi_{ij}^{\mu\nu})^2 \right]_{\text{av}} e^{ik(i-j)}, \quad (8)$$

where

$$\chi_{ij}^{\mu\nu} = \langle S_i^\mu S_j^\nu \rangle - \langle S_i^\mu \rangle \langle S_j^\nu \rangle. \quad (9)$$

From it the spin glass correlation length  $\xi_{\text{SG}}$  is then determined using the relation

$$\xi_{\text{SG}} = \frac{1}{2 \sin(k_{\min}/2)} \left( \frac{\chi_{\text{SG}}(0)}{\chi_{\text{SG}}(k_{\min})} - 1 \right)^{1/(2\sigma-1)}. \quad (10)$$

$k_{\min} = 2\pi/N$  is the smallest non-zero wavevector compatible with the boundary conditions. The spin glass susceptibility  $\chi_{\text{SG}} = \chi_{\text{SG}}(0)$ .

We have studied  $\xi_{\text{SG}}$  as a function of  $h_r$  at temperature  $T = 0.241$  for  $\sigma = 0.75$ , and for  $\sigma = 0.85$  at  $T = 0.112$ , so that for both values of  $\sigma$ ,  $T/T_c \approx 0.67$ .  $T_c$  is the zero field transition temperature, which for  $\sigma = 0.75$  is  $0.359 \pm 0.005$  and for  $\sigma = 0.85$  is  $0.166 \pm 0.004$ , according to [39]. It is possible to study much larger systems for  $\sigma = 0.75$  than for  $\sigma = 0.85$  at  $T/T_c = 0.67$  as the  $T_c$  is smaller at  $\sigma = 0.85$  and equilibration of the system is easier at higher temperatures. We shall now describe the field dependence of  $\xi_{\text{SG}}$  according to the droplet picture [12, 13, 47], including also the finite size modifications, and compare these with our simulation data. We discount the possibility of an AT transition at these values of  $\sigma$  [16, 48].

In the droplet picture one uses an Imry-Ma argument [49] for the correlation length  $\xi$  and identifies it with the size of the region or domain within which the spins become re-oriented in the presence of the random field. The free energy gained from such a reorientation by the the random field is of order  $\sqrt{q_{\text{EA}}(T)} h_r \xi^{d/2}$ . The size of such domains  $\xi$  is determined by equating this free energy to the free energy cost of the interface of this domain of re-ordered spins with the rest of the system, which is of

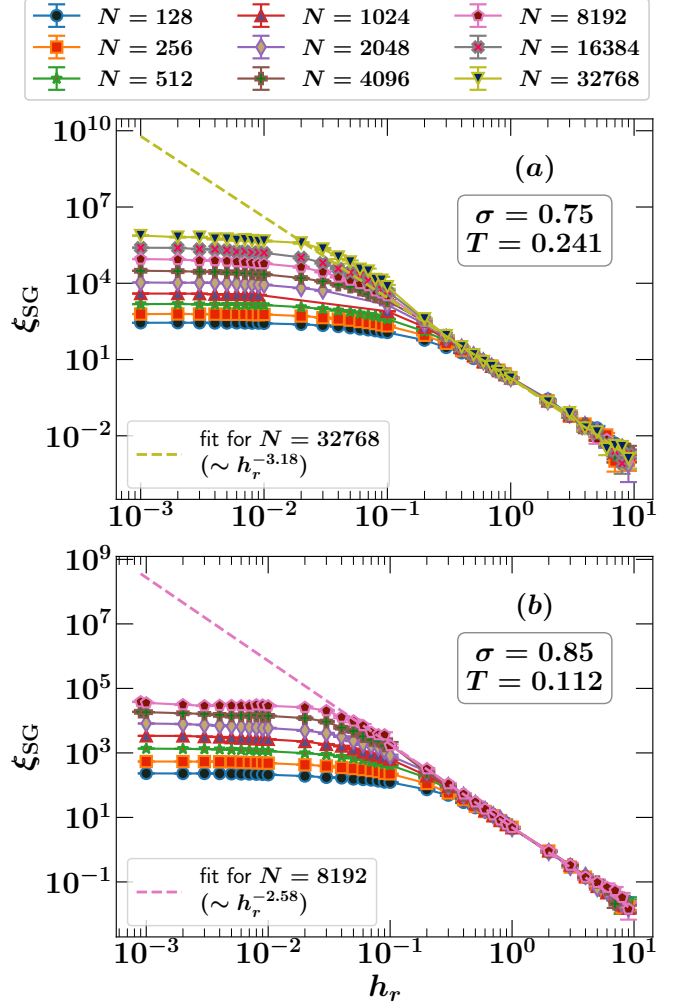


FIG. 1. Plots of  $\xi_{\text{SG}}$  versus  $h_r$  for (a)  $\sigma = 0.75$  and (b)  $\sigma = 0.85$ , for a range of system sizes  $N$ . When  $\xi_{\text{SG}} \ll N$  the plots become  $N$  independent, as  $\xi_{\text{SG}} \sim 1/h_r^x$ . For  $\sigma = 0.75$ ,  $x$  is close to 3.18, while for  $\sigma = 0.85$ ,  $x$  is close to 2.58 (see Table II).

the form  $\Upsilon(T)\xi^{\theta'}$  [50]. Equating these two free energies gives

$$\xi \sim \left[ \frac{\Upsilon(T)}{\sqrt{q_{\text{EA}}(T)} h_r} \right]^x, \quad (11)$$

where

$$x = \frac{1}{d/2 - \theta'}. \quad (12)$$

While there is a considerable literature on the dependence of the interface exponent  $\theta'$  on  $\sigma$  for the case of Ising spin glasses [51], the case of the Heisenberg spin glass has hardly been studied. Eq. (11) shows that as  $h_r \rightarrow 0$ , the length scale becomes infinite;  $\xi$  diverges as  $\xi \sim 1/h_r^x$ . We would expect this formula to apply until finite size effects limit its growth, which will occur when  $\xi$  is of  $O(L)$  (or  $O(N)$  in our one-dimensional system).



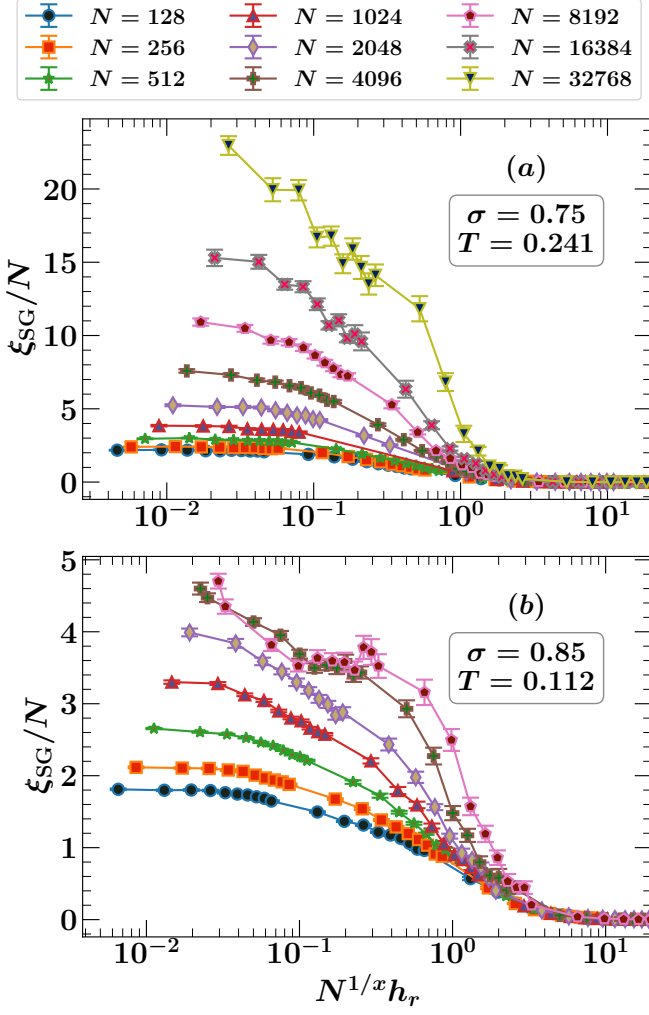


FIG. 2. Plots of  $\xi_{\text{SG}}/N$  versus  $h_r N^{1/x}$  on a log-linear scale for (a)  $\sigma = 0.75$  and (b)  $\sigma = 0.85$ . Note that for the two largest sizes at  $\sigma = 0.85$  the lines are running close together, suggesting that they are in the region where  $L > L^*$ , but a similar effect is not visible at  $\sigma = 0.75$ , which suggests that in this case  $L^*$  is larger than the largest system studied at this value of  $\sigma$ .

Identifying  $\xi_{\text{SG}}$  with  $\xi$ , Fig. 1 shows that the Imry-Ma fit indeed works well at the larger fields for both values of  $\sigma$ ; the data for the larger  $h_r$  collapse nicely onto a power law form as predicted by Eq. (11) for all sizes  $N$ . It only departs from this formula when  $\xi_{\text{SG}}$  becomes of order  $N$ , when finite size corrections to the Imry-Ma formula are needed. TNT effects produce corrections to the Imry-Ma formula when  $\xi_{\text{SG}}$  is of  $O(N)$  unless  $N = L > L^*$ . But for values of  $\xi_{\text{SG}}$  of the order of just a few lattice spacings, droplet scaling expectations work very well, just as was also observed for the case of temperature chaos when the chaos length scale was of the order of a few lattice spacings [35].

The conventional finite size scaling form for corrections

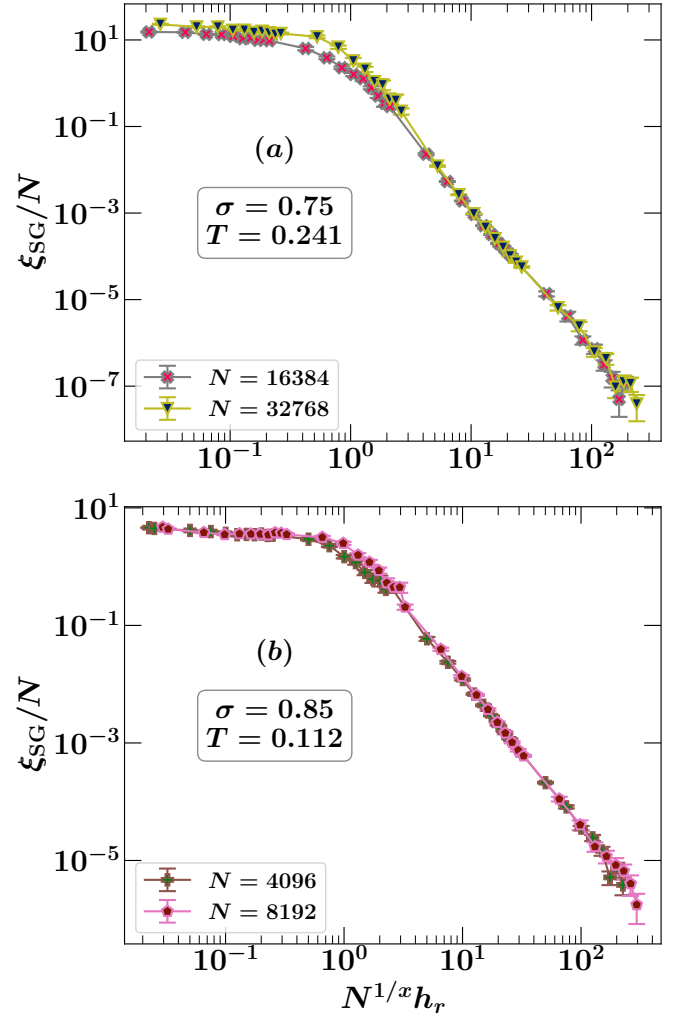


FIG. 3. Plots of  $\xi_{\text{SG}}/N$  versus  $h_r N^{1/x}$  on a log-log scale for (a)  $\sigma = 0.75$  and (b)  $\sigma = 0.85$  for the two largest sizes available at each value of  $\sigma$ . For  $\sigma = 0.85$  the lines are running close together, suggesting that they are in the region where  $L > L^*$ , and that the data at these sizes has the finite size scaling form of Eq. (13). At  $\sigma = 0.75$  the curves have not run together in the region where  $\xi_{\text{SG}}/N$  is of  $O(1)$ , which suggests that in this case  $L^*$  is larger than the largest system studied and that the finite size form of Eq. (13) is not yet applicable.

to the scaling of Eq. (11) would be of the form

$$\frac{\xi_{\text{SG}}}{N} = \mathcal{X}(N^{1/x} h_r) + N^{-\omega} \mathcal{H}(N^{1/x} h_r), \quad (13)$$

where  $\omega$  is the correction to scaling exponent, but for the fact that TNT effects produce large further corrections to these asymptotic forms, at least when  $L < L^*$ . As a scaling form Eq. (13) should hold at fixed values of  $h_r N^{1/x}$  as  $N \rightarrow \infty$ . Since in our studies  $L^*$  is probably larger than the length  $N$  of our system, at least for  $\sigma = 0.75$ , the scaling form of Eq. (13) does not work in the region where  $\xi_{\text{SG}}$  is of order  $N$ . In Fig. 2 we have plotted  $\xi_{\text{SG}}/N$  against  $h_r N^{1/x}$  on a log-linear plot (which better reveals departures from scaling) to check the validity of

TABLE I. The table provides the parameters for simulations performed at a fixed temperature  $T$  with varying field values  $h_r$ .  $N(h_r)$  denotes the number of field values sampled within the range  $h_r(\text{min,max})$ . Equilibration times differ based on the field values and fall within the range  $N_{\text{sweep}}(\text{min,max})$ . The number of disorder samples collected for various field values is indicated by  $N_{\text{samp}}(\text{min,max})$ .  $t_{\text{tot}}$  represents the total CPU time (in hours) required to generate data for each system size. The computation time reflects the total duration needed to obtain all the data using a single core with an average clock speed of 2.6 GHz. During the measurement phase, one measurement was taken every four sweeps.

$\sigma$	$T$	$N$	$h_r(\text{min,max})$	$N(h_r)$	$N_{\text{sweep}}(\text{min,max})$	$N_{\text{samp}}(\text{min,max})$	$t_{\text{tot}}(\text{hrs})$
0.750	0.241	128	(0.0010, 9.0000)	36	(256, 2048)	(4000, 16000)	5.03
0.750	0.241	256	(0.0010, 9.0000)	36	(512, 4096)	(4000, 16000)	19.67
0.750	0.241	512	(0.0010, 9.0000)	36	(1024, 8192)	(4000, 14000)	77.83
0.750	0.241	1024	(0.0010, 9.0000)	27	(2048, 16384)	(1600, 14000)	66.30
0.750	0.241	2048	(0.0010, 9.0000)	30	(4096, 32768)	(2000, 14000)	391.68
0.750	0.241	4096	(0.0010, 9.0000)	36	(8192, 1048576)	(1600, 15000)	8171.79
0.750	0.241	8192	(0.0010, 9.0000)	36	(16384, 4194304)	(663, 12800)	40361.13
0.750	0.241	16384	(0.0010, 9.0000)	36	(32768, 8388608)	(240, 24725)	129968.71
0.750	0.241	32768	(0.0010, 9.0000)	36	(65536, 2097152)	(240, 15280)	326476.90
0.850	0.112	128	(0.0010, 9.0000)	36	(2048, 8192)	(8000, 8000)	18.58
0.850	0.112	256	(0.0010, 9.0000)	36	(4096, 524288)	(4000, 18000)	1166.46
0.850	0.112	512	(0.0010, 9.0000)	36	(4096, 1048576)	(2400, 20000)	6668.51
0.850	0.112	1024	(0.0010, 9.0000)	36	(16384, 4194304)	(2100, 16000)	30521.51
0.850	0.112	2048	(0.0010, 9.0000)	36	(65536, 8388608)	(720, 22400)	86440.89
0.850	0.112	4096	(0.0009, 9.0000)	37	(32768, 16777216)	(300, 39200)	294691.75
0.850	0.112	8192	(0.0009, 9.0000)	37	(32768, 16777216)	(447, 42946)	573696.81

Eq. (13) for values of the variable  $h_r N^{1/x}$  less than 10. For both values of  $\sigma$  there are clear departures from the scaling form which we attribute to TNT effects which arise in the region where  $\xi_{\text{SG}} \sim N$ . However, for  $\sigma = 0.85$  where  $L^*$  is expected to be smaller than for  $\sigma = 0.75$ , Fig. 2 hints that Eq. (13) might apply as the plots at adjacent sizes for the larger  $N$  values seem to be getting closer together as  $N$  is increased (which is a feature predicted by Eq. (13)). The contrasting behaviors for  $\sigma = 0.75$  and  $\sigma = 0.85$  for the two largest system sizes at each value of  $\sigma$  is displayed in Fig. 3 on a log-log plot so that we can display behavior for all the values of  $h_r N^{1/x}$  which we have studied. We see in Fig. 3 that at  $h_r N^{1/x}$  around unity, Eq. (13) does seem to apply as  $N$  becomes larger than 4000 for the case of  $\sigma = 0.85$ . However, for the case when  $\sigma = 0.75$ , where we expect  $L^*$  to be larger than for  $\sigma = 0.85$ , we do not seem to have reached system sizes  $N$  where droplet scaling will apply.

One complication that we have not discussed is that the scaling form of Eq. (13) will not apply for very small values of the field  $h_r$ . It is implicit in this equation that the field  $h_r$  is sufficiently large so that, for example, the Parisi overlap function  $P(q)$  is zero for  $q < 0$ . This requires that  $h_r \sqrt{q_{\text{EA}} N} \gg T$ . Plots of  $P(q)$  in fields  $h_r$  of  $O(1/\sqrt{N})$  can be found in Ref. [52]. The argument of the crossover function  $h_r N^{1/x}$  at the point of just satisfying the inequality is of  $O(N^{(1/x-1/2)})$  which is small at large  $N$  since  $x > 2$ . In other words, the scaling form of Eq. (13) should hold on the droplet picture for any finite value of  $h_r N^{1/x}$  provided  $N$  is large enough. Any departures from Eq. (13) at the largest sizes we have studied

seem unlikely to be caused by the small field effect. The failure to obey droplet scaling forms at  $\sigma = 0.75$  seems more likely to be connected with TNT effects than with using too small values of  $h_r$ , as  $x$  is larger for this value of  $\sigma$  than for  $\sigma = 0.85$ , so it should be *easier* to satisfy the criterion on  $h_r$  for this case. Hence it seems likely the TNT effects are the cause of the poor scaling collapse in Fig. 2 for  $\sigma = 0.75$ , rather than being caused by using too small values of  $h_r$ .

We have also studied the behavior of  $\chi_{\text{SG}}$  as a function of  $N$ ,  $h_r$  and  $\sigma$  but have relegated its analysis to Appendix A because it involves an additional fitting parameter,  $z$ , making it less straightforward than the case of  $\xi_{\text{SG}}$ . Its behavior though is very similar to that found for  $\xi_{\text{SG}}$ .

### III. ORIGIN OF TNT BEHAVIOR AS A FINITE SIZE EFFECT

We shall now explain using conventional renormalization group (RG) arguments the origin of TNT as a finite size effect. Our system has a correlation length  $\xi_{\text{SG}}$  which becomes large at small values of  $h_r$ . When there is a long correlation length there is scope for an RG approach. Our simulations show that when the field is sufficiently small so  $\xi_{\text{SG}}$  is of order  $L$  then TNT effects are visible and only get small again if  $L > L^*(T, \sigma)$ , where  $L^*$  is a large length. Our results in Figs. 2 and 3 suggest that  $L^*$  for  $\sigma = 0.85$  is in the range  $L^* \sim 4000 - 8000$ , while for  $\sigma = 0.75$  all we can say is that its  $L^*$

TABLE II. Values of the exponents  $x_\chi$ ,  $x$ , and  $z$  derived from our simulations for various values of  $\sigma$  and temperature  $T$ . For Heisenberg spins the values of these exponents are obtained from the fitting procedure shown in Figs. 1 and A1. The corresponding values of the exponents for XY spins are obtained from Fig. 9 in [43].

	$\sigma$	$T$	$T_c$	$T/T_c$	$x_\chi$	$x$	$z$
XY	0.75	0.55	0.62	0.89	$1.6114 \pm 0.0005$	$2.7077 \pm 0.0531$	$0.5951 \pm 0.0119$
XY	0.85	0.3	0.33	0.91	$1.8919 \pm 0.0014$	$2.2019 \pm 0.0152$	$0.8592 \pm 0.0066$
Heisenberg	0.75	0.241	0.359	0.671	$1.8926 \pm 0.0003$	$3.1790 \pm 0.0730$	$0.5954 \pm 0.0138$
Heisenberg	0.85	0.112	0.166	0.674	$2.1322 \pm 0.0011$	$2.5822 \pm 0.0387$	$0.8257 \pm 0.0128$

is greater than the largest system we could study, which was  $N = 32768$ .

As  $h_r \rightarrow 0$ ,  $\xi_{SG}$  will approach the zero-field cumulant correlation length, which is of order  $L$ . This is the origin of the flattening off of  $\xi_{SG}/N$  in Fig. 3 as  $N^{1/x}h_r$  goes to zero. When  $T < T_c$ , the system at  $h_r = 0$  is in the low-temperature phase of the zero-field spin glass. The RG flows will take the system to its zero-temperature fixed point. In fact the exponent  $\theta'$  which determines  $x$  is an exponent of the zero temperature fixed point in zero-field; it is not associated with the critical fixed point. In the presence of a non-zero value of  $h_r$ , we expect the RG flows to be towards this fixed point, and veering away from it before it is reached:  $h_r$  is a relevant perturbation at the zero-temperature fixed point.

Under the RG flow, the coupling constants of its field theory will be flowing towards the values which they take at this (stable) zero-temperature fixed point (at  $h_r = 0$ ). There are, of course, a large number of such coupling constants but we will just focus on one of them, the renormalized temperature  $T(l)$ . Once  $\xi_{SG}$  becomes comparable to its zero field cumulant value then we shall use the strategy used by Brézin and Zinn-Justin [28] of reducing the field theory to just the  $q_{\alpha\beta}(k = 0)$  mode. (We are envisaging the use of periodic boundary conditions). The gradient terms now disappear from the field theory and the remaining integrals over the  $q_{\alpha\beta}$  are then of the same form as is encountered in the mean-field Sherrington-Kirkpatrick (SK) model [20]. Hence provided one only looks at features which involve this mode one will see all the features normally seen in that model such as many states with an ultrametric topology, excitations which are of  $O(1)$  and so on. The neglected modes of non-zero wavevector make a sub-dominant contribution to the finite size scaling functions. The Parisi overlap function  $P(q)$ , which is a function of  $q_{\alpha\beta}(k = 0)$ , naturally will have features similar to those seen in the SK model. It is natural therefore that there will exist excitations on the scale of the system size  $L$  whose free energies are of  $O(1)$  with fractal dimension  $d_s = d$ , just as was envisaged by Houdayer and Martin [9], who did not make use of any RG argument in making their suggestions.

The value to be used for  $T(l)$  is its value at which the RG length scale, which grows as  $e^l$ , reaches the system size  $L$ . At this point mean-field theory will be useful provided  $L$  itself is large enough so that the modes  $q_{\alpha\beta}(k)$

with  $k$  non-zero can be ignored. It is only for an infinite system in zero field that the coupling constants reach their fixed point values and  $T(l)$  becomes zero. Thus it would seem natural that many of the features associated with the replica symmetry breaking results of Parisi should appear to be present in low-dimensional spin glasses, even though they are essentially present because of these finite size effects. A pronounced change in behavior once the correlation length becomes of order of the size of the system was found in the numerical work of [53].

For very large systems, the effective temperature  $T(l)$  will get very close to zero. Then the argument of Crisanti and de Dominicis [54, 55] will come into play. They observed that in the SK model as  $T \rightarrow 0$  the Parisi overlap function  $q(x)$  becomes nearly independent of  $x$  (until  $x \sim T$  when it starts to fall almost linearly to zero as  $x \rightarrow 0$ ). In other words, it is becoming nearly replica symmetric at low-temperatures.  $q(x)$  is expected on the droplet picture to be independent of  $x$ . It has replica symmetry, i.e. constant  $q(x)$ . For  $L > L^*$  one has reached effective temperatures  $T(l)$  so small that one is in the region studied in Refs. [54, 55]. In this limit, the zero-field Parisi overlap function  $P(q)$  at  $q = 0$  will decrease as  $T/L^{\theta'}$ , the form expected in the droplet picture [13, 56].  $L^*$  is not associated with any sharp features but marks the system size above which droplet features dominate the behavior.

Of course it would be useful if we could demonstrate explicitly these RG features by direct calculation. For the much simpler problem of the  $\phi^4$  scalar field theory such a program of using RG calculations to explore finite size features was done in Ref. [57]. Alas for spin glasses we do not have well-founded RG equations for the low-temperature phase although we have RG equations for the critical behavior in zero field [58, 59]. There are real space RG equations like the Migdal-Kadanoff approximation but they are not consistent with the existence of many pure states [60] and do not produce TNT features, as was found long ago [56] for temperatures  $T$  well below  $T_c$ . For the Migdal-Kadanoff RG procedure there is no sign of a large length scale like  $L^*$ ; one quickly reaches asymptopia. It would therefore be useful if RG equations could be found which would reach asymptopia only when  $L > L^*$ , with  $L^*$  being a large length scale.

While no such RG calculation is known to us, Middle-

ton [22] (see also Ref. [61]) predicted that it would only be at very large values of  $L$  that the decay of the Parisi overlap function  $P(q)$  at  $q = 0$  would be as  $T/L^{\theta'}$  (the form predicted by droplet scaling); for smaller systems it would appear to be almost  $L$  independent. It would be interesting to understand in detail how finite size effects produce droplets of free energy  $O(1)$  which are of the size of the system  $L$  in order to account for the TNT behavior [9]. In two dimensions we have already mentioned that droplets are strongly affected by finite size effects (whilst domain walls are not) [23–25, 27].

#### IV. SUMMARY AND CONCLUSIONS

In this paper, we addressed the long-standing debate regarding the nature of the ordered state in spin glasses, focusing on four major theoretical frameworks: the replica symmetry breaking (RSB) picture, the chaotic pairs state, the TNT picture, and the droplet scaling picture. Using a detailed simulation study of a one-dimensional spin glass proxy model, we aimed to clarify the nature of the ordered state. Specifically, we investigated the droplet scaling and TNT pictures, where finite size effects often obscure the true behavior of the system. By studying large system sizes, we observed that TNT-like features, fade away when the system exceeds a critical length scale  $L^*$ . These findings suggest that the TNT-like effects are artifacts of finite size rather than being indicative of the true nature of the ordered state. Our results thus provide evidence in favor of the droplet scaling picture as the correct description of the ordered state in low-dimensional systems, such as  $d = 3$ , while highlighting the role of finite size effects in spin glass simulations.

In our simulations, we utilized a one-dimensional proxy model to investigate two values of  $\sigma > 2/3$ :  $\sigma = 0.75$  and  $\sigma = 0.85$ . The temperature was held constant at approximately  $0.67 T_c$ , while the magnetic field was varied to generate data for each  $\sigma$  value. For  $\sigma = 0.75$ , the largest system size considered was  $N = 32768$ , and for  $\sigma = 0.85$ , we studied systems up to  $N = 8192$ , surpassing the maximum system size ( $N = 4096$ ) analyzed in [43] for  $\sigma = 0.85$ . Our findings, illustrated in Figs. 2 and 3, exhibit a notable data collapse for  $\sigma = 0.85$ , attributed to the fact that the largest system size  $L$  exceeds the critical value  $L^*$  for this  $\sigma$ . However, for  $\sigma = 0.75$ , this collapse was not observed, as the system sizes explored in this study remain within the regime where  $L < L^*$ .

Our numerical results showed that TNT effects appear when  $\xi_{SG} \sim L$ , provided  $L < L^*$ . These effects vanish when  $L > L^*$ . A remaining challenge therefore is to develop detailed RG calculations that explain the emergence of the  $L^*$  feature. These would hopefully at the same time explain why there appears to be no AT line below six dimensions [16] and describe the dimensionality and temperature dependence of  $L^*$ . Alas, RG calculations in the ordered phase of spin glasses are very

challenging. In particular we know of no RG calculation which gives a large  $L^*$ .

The scenario outlined in this paper gives an important role to RSB and TNT features in three dimensional spin glasses when  $L < L^*$ . Because  $L^*$  is such a large length it seems likely that no simulation has ever been done in three dimensions with  $L > L^*$ . Alas the actual value of  $L^*$  for the three dimensional Ising spin glass remains unknown.

#### ACKNOWLEDGMENTS

We thank D. L. Stein and A. P. Young for valuable exchanges. We are grateful to the High Performance Computing (HPC) facility at IISER Bhopal, where large-scale calculations in this project were run. B.V is grateful to the Council of Scientific and Industrial Research (CSIR), India, for his PhD fellowship. A.S acknowledges financial support from SERB via the grant (File Number: CRG/2019/003447), and from DST via the DST-INSPIRE Faculty Award [DST/INSPIRE/04/2014/002461].

#### Appendix A: Spin glass susceptibility

The spin glass susceptibility is predicted by the droplet picture to be of the form [43]

$$\frac{\chi_{SG}}{N^z} = \mathcal{C}(N^{1/x} h_r) + N^{-\omega} \mathcal{G}(N^{1/x} h_r), \quad (\text{A1})$$

where the crossover function  $\mathcal{C}(y) \sim 1/y^{x_\chi}$  for large  $y$ , leading to  $\chi_{SG} \sim \xi^z$  and becoming independent of  $N$ . In this regime, the susceptibility scales as

$$\chi_{SG} \sim 1/h_r^{x_\chi}, \quad (\text{A2})$$

implying the relationship  $x_\chi = xz$ . For small  $y$ ,  $\mathcal{C}(y)$  approaches a constant value. Our results, shown in Figs. A1(a) and A1(b), confirm that  $\chi_{SG}$  collapses onto a power law as predicted by this form, for all system sizes  $N$  when  $h_r$  is large. The exponent  $z$  must be determined by fitting the data (see Ref. [43] for a detailed discussion of these exponents). Our results for the droplet exponents  $x$ ,  $x_\chi$ , and  $z$  for  $\sigma = 0.75$  and  $\sigma = 0.85$  are summarized in Table II for both the XY and Heisenberg models.

The data collapse is shown in Figs. A2(a) and A2(b). We determine  $z$  by noting that when  $N^{1/x} h_r$  is large,  $\chi_{SG}$  becomes independent of  $N$ . Remarkably, the value of  $z$ , which fits well at large  $N^{1/x} h_r$ , also provides a good collapse for small  $N^{1/x} h_r$ . The distinct behaviors for  $\sigma = 0.75$  and  $\sigma = 0.85$  at the largest system sizes are evident in Fig. A3, displayed on a log-log plot to show behavior across all values of  $h_r N^{1/x}$  studied. Corrections to the Imry-Ma scaling form are very noticeable, in particular in Fig. A2(a) for small  $N^{1/x} h_r$ , similar to the behavior in the  $\xi_{SG}$  plot, Fig. 2(a), which are both for  $\sigma = 0.75$ , and due to TNT effects.



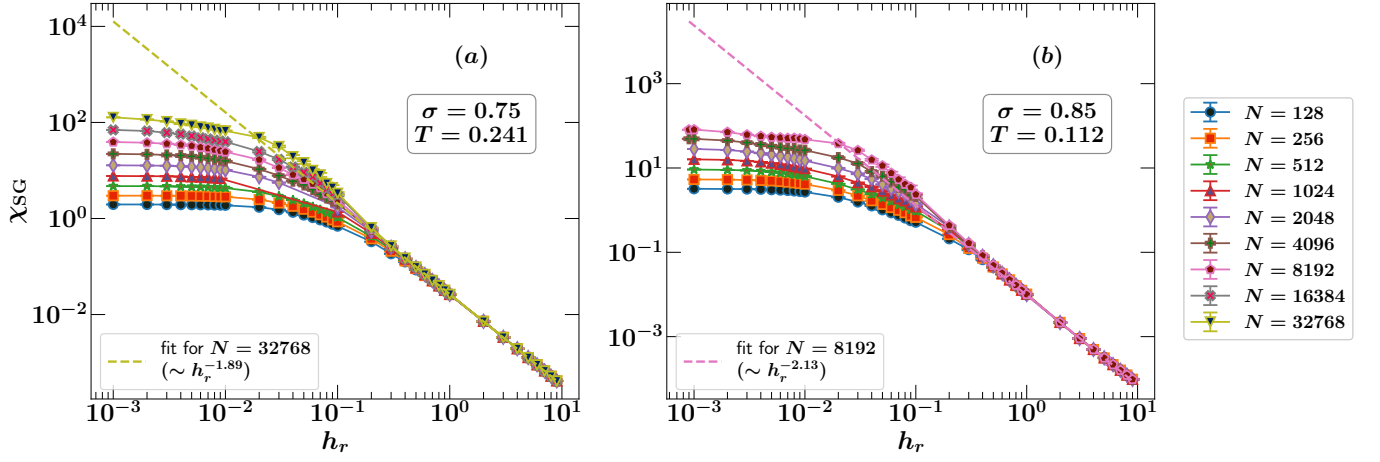


FIG. A1. Log-log plots of  $\chi_{\text{SG}}$  as a function of  $h_r$  for (a)  $\sigma = 0.75$  and (b)  $\sigma = 0.85$ , shown for various system sizes  $N$ . At higher values of  $h_r$ , the curves converge, indicating that  $\chi_{\text{SG}}$  becomes independent of  $N$ , following the scaling behavior  $\chi_{\text{SG}} \sim 1/h_r^{x_\chi}$ . For  $\sigma = 0.75$ ,  $x_\chi$  is approximately 3.18, while for  $\sigma = 0.85$ ,  $x_\chi$  is around 2.58 (see Table II).

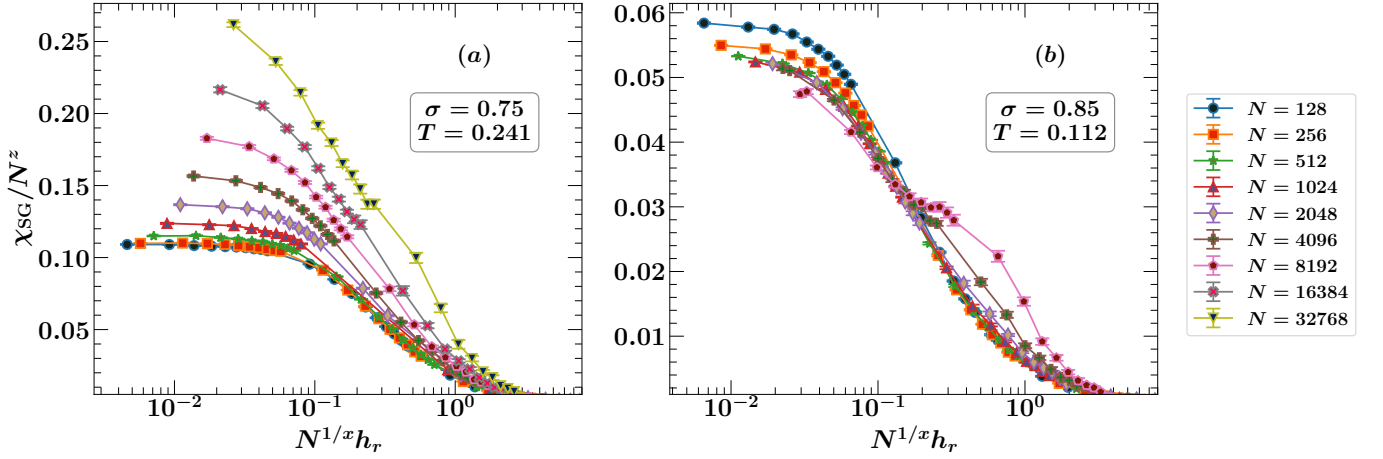


FIG. A2. Plots of  $\chi_{\text{SG}}/N^z$  against  $h_r N^{1/x}$  on a log-linear scale for (a)  $\sigma = 0.75$  and (b)  $\sigma = 0.85$ , illustrating the scaling behavior across different system sizes.

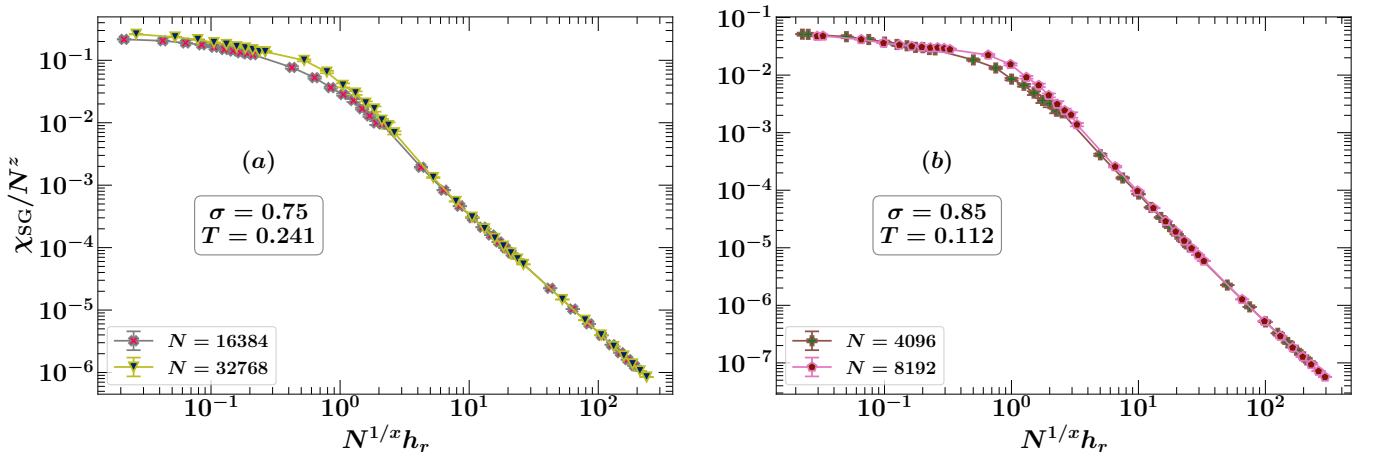


FIG. A3. Plots of  $\chi_{\text{SG}}/N^z$  versus  $h_r N^{1/x}$  on a log-log scale for (a)  $\sigma = 0.75$  and (b)  $\sigma = 0.85$ , showcasing the behavior for the two largest system sizes available at each  $\sigma$  value.

- 
- [1] C. M. Newman and Stein D.L., “Finite-Dimensional Spin Glasses: States, Excitations, and Interfaces,” *Annales Henri Poincaré* **4**, 497 (2003).
- [2] G. Parisi, “Toward a mean field theory for spin glasses,” *Physics Letters A* **73**, 203–205 (1979).
- [3] Giorgio Parisi, “Order Parameter for Spin-Glasses,” *Phys. Rev. Lett.* **50**, 1946–1948 (1983).
- [4] R. Rammal, G. Toulouse, and M. A. Virasoro, “Ultrametricity for physicists,” *Rev. Mod. Phys.* **58**, 765–788 (1986).
- [5] Marc Mézard, Giorgio Parisi, and Miguel Angel Virasoro, *Spin glass theory and beyond: An Introduction to the Replica Method and Its Applications*, Vol. 9 (World Scientific Publishing Company, 1986).
- [6] Giorgio Parisi, “Some considerations of finite-dimensional spin glasses,” *Journal of Physics A: Mathematical and Theoretical* **41**, 324002 (2008).
- [7] C. M. Newman and D. L. Stein, “Simplicity of state and overlap structure in finite-volume realistic spin glasses,” *Phys. Rev. E* **57**, 1356–1366 (1998).
- [8] Matteo Palassini and A. P. Young, “Nature of the Spin Glass State,” *Phys. Rev. Lett.* **85**, 3017–3020 (2000).
- [9] J. Houdayer and O. C. Martin, “A geometrical picture for finite-dimensional spin glasses,” *Europhysics Letters* **49**, 794 (2000).
- [10] F. Krzakala and O. C. Martin, “Spin and Link Overlaps in Three-Dimensional Spin Glasses,” *Phys. Rev. Lett.* **85**, 3013–3016 (2000).
- [11] W L McMillan, “Scaling theory of Ising spin glasses,” *Journal of Physics C: Solid State Physics* **17**, 3179 (1984).
- [12] A. J. Bray and M. A. Moore, “Scaling Theory of the ordered phase of spin glasses,” in *Heidelberg Colloquium on Glassy Dynamics and Optimization*, edited by L. Van Hemmen and I. Morgenstern (Springer, New York, 1986) p. 121.
- [13] Daniel S. Fisher and David A. Huse, “Equilibrium behavior of the spin-glass ordered phase,” *Phys. Rev. B* **38**, 386–411 (1988).
- [14] Mutian Shen, Gerardo Ortiz, Yang-Yu Liu, Martin Weigel, and Zohar Nussinov, “Universal Fragility of Spin Glass Ground States under Single Bond Changes,” *Phys. Rev. Lett.* **132**, 247101 (2024).
- [15] J R L de Almeida and D J Thouless, “Stability of the Sherrington-Kirkpatrick solution of a spin glass model,” *Journal of Physics A: Mathematical and General* **11**, 983 (1978).
- [16] Bharadwaj Vedula, M. A. Moore, and Auditya Sharma, “Evidence that the AT transition disappears below six dimensions,” (2024), [arXiv:2402.03711 \[cond-mat.dis-nn\]](https://arxiv.org/abs/2402.03711).
- [17] R Alvarez Baños, A Cruz, L A Fernandez, J M Gil-Narvion, A Gordillo-Guerrero, M Guidetti, A Maiorano, F Mantovani, E Marinari, V Martin-Mayor, J Monforte-Garcia, A Muñoz Sudupe, D Navarro, G Parisi, S Perez-Gaviro, J J Ruiz-Lorenzo, S F Schifano, B Seoane, A Tarancon, R Tripiccion, and D Yllanes, “Nature of the spin-glass phase at experimental length scales,” *Journal of Statistical Mechanics: Theory and Experiment* **2010**, P06026 (2010).
- [18] T. Aspelmeier, M. A. Moore, and A. P. Young, “Interface Energies in Ising Spin Glasses,” *Phys. Rev. Lett.* **90**, 127202 (2003).
- [19] T. Aspelmeier, Wenlong Wang, M. A. Moore, and Helmut G. Katzgraber, “Interface free-energy exponent in the one-dimensional Ising spin glass with long-range interactions in both the droplet and broken replica symmetry regions,” *Phys. Rev. E* **94**, 022116 (2016).
- [20] David Sherrington and Scott Kirkpatrick, “Solvable Model of a Spin-Glass,” *Phys. Rev. Lett.* **35**, 1792–1796 (1975).
- [21] M. A. Moore, “Droplet-scaling versus replica symmetry breaking debate in spin glasses revisited,” *Phys. Rev. E* **103**, 062111 (2021).
- [22] A. Alan Middleton, “Extracting thermodynamic behavior of spin glasses from the overlap function,” *Phys. Rev. B* **87**, 220201 (2013).
- [23] Hamid Khoshbakht and Martin Weigel, “Domain-wall excitations in the two-dimensional Ising spin glass,” *Phys. Rev. B* **97**, 064410 (2018).
- [24] A. K. Hartmann and M. A. Moore, “Corrections to scaling are large for droplets in two-dimensional spin glasses,” *Phys. Rev. Lett.* **90**, 127201 (2003).
- [25] A. K. Hartmann and M. A. Moore, “Generating droplets in two-dimensional Ising spin glasses using matching algorithms,” *Phys. Rev. B* **69**, 104409 (2004).
- [26] A J Bray and M A Moore, “Lower critical dimension of Ising spin glasses: a numerical study,” *Journal of Physics C: Solid State Physics* **17**, L463 (1984).
- [27] A. K. Hartmann and A. P. Young, “Metastate analysis of the ground states of two-dimensional Ising spin glasses,” *Phys. Rev. E* **108**, 024142 (2023).
- [28] E. Brézin and J. Zinn-Justin, “Finite size effects in phase transitions,” *Nuclear Physics B* **257**, 867–893 (1985).
- [29] A J Bray and M A Moore, “Finite size effects in spin glass overlap functions,” *Journal of Physics A: Mathematical and General* **18**, L683 (1985).
- [30] A. J. Bray and M. A. Moore, “Chaotic Nature of the Spin-Glass Phase,” *Phys. Rev. Lett.* **58**, 57–60 (1987).
- [31] T. Aspelmeier, A. J. Bray, and M. A. Moore, “Why Temperature Chaos in Spin Glasses Is Hard to Observe,” *Phys. Rev. Lett.* **89**, 197202 (2002).
- [32] Matteo Palassini and A. P. Young, “Nature of the spin glass state,” *Phys. Rev. Lett.* **85**, 3017–3020 (2000).
- [33] Helmut G. Katzgraber, Matteo Palassini, and A. P. Young, “Monte Carlo simulations of spin glasses at low temperatures,” *Phys. Rev. B* **63**, 184422 (2001).
- [34] Stefan Boettcher, “Physics of the Edwards-Anderson Spin Glass in Dimensions  $d = 3, \dots, 8$  from Heuristic Ground State Optimization,” (2024), [arXiv:2407.14646 \[cond-mat.dis-nn\]](https://arxiv.org/abs/2407.14646).
- [35] Helmut G. Katzgraber and Florent Krzakala, “Temperature and Disorder Chaos in Three-Dimensional Ising Spin Glasses,” *Phys. Rev. Lett.* **98**, 017201 (2007).
- [36] Giorgio Parisi and Tommaso Rizzo, “Chaos in temperature in diluted mean-field spin-glass,” *Journal of Physics A: Mathematical and Theoretical* **43**, 235003 (2010).
- [37] Helmut G. Katzgraber and A. P. Young, “Monte Carlo studies of the one-dimensional Ising spin glass with power-law interactions,” *Phys. Rev. B* **67**, 134410 (2003).
- [38] L. Leuzzi, G. Parisi, F. Ricci-Tersenghi, and J. J. Ruiz-Lorenzo, “Dilute One-Dimensional Spin Glasses with Power Law Decaying Interactions,” *Phys. Rev. Lett.* **101**, 107203 (2008).

- [39] Auditya Sharma and A. P. Young, “Phase transitions in the one-dimensional long-range diluted Heisenberg spin glass,” *Phys. Rev. B* **83**, 214405 (2011).
- [40] Dao Xuan Viet and Hikaru Kawamura, “Spin-Chirality Decoupling in the One-Dimensional Heisenberg Spin Glass with Long-Range Power-Law Interactions,” *Phys. Rev. Lett.* **105**, 097206 (2010).
- [41] Auditya Sharma and A. P. Young, “de Almeida–Thouless line in vector spin glasses,” *Phys. Rev. E* **81**, 061115 (2010).
- [42] L. W. Lee and A. P. Young, “Large-scale Monte Carlo simulations of the isotropic three-dimensional Heisenberg spin glass,” *Phys. Rev. B* **76**, 024405 (2007).
- [43] Bharadwaj Vedula, M. A. Moore, and Auditya Sharma, “Study of the de Almeida–Thouless line in the one-dimensional diluted power-law  $XY$  spin glass,” *Phys. Rev. E* **108**, 014116 (2023).
- [44] R. A. Baños, L. A. Fernandez, V. Martin-Mayor, and A. P. Young, “Correspondence between long-range and short-range spin glasses,” *Phys. Rev. B* **86**, 134416 (2012).
- [45] J. H. Pixley and A. P. Young, “Large-scale Monte Carlo simulations of the three-dimensional  $XY$  spin glass,” *Phys. Rev. B* **78**, 014419 (2008).
- [46] Helmut G. Katzgraber, Matteo Palassini, and A. P. Young, “Monte Carlo simulations of spin glasses at low temperatures,” *Phys. Rev. B* **63**, 184422 (2001).
- [47] W L McMillan, “Scaling theory of Ising spin glasses,” *Journal of Physics C: Solid State Physics* **17**, 3179–3187 (1984).
- [48] Helmut G. Katzgraber and A. P. Young, “Probing the Almeida–Thouless line away from the mean-field model,” *Phys. Rev. B* **72**, 184416 (2005).
- [49] Yoseph Imry and Shang-keng Ma, “Random-Field Instability of the Ordered State of Continuous Symmetry,” *Phys. Rev. Lett.* **35**, 1399–1401 (1975).
- [50] T. Aspelmeier, Helmut G. Katzgraber, Derek Larson, M. A. Moore, Matthew Wittmann, and Joonhyun Yeo, “Finite-size critical scaling in Ising spin glasses in the mean-field regime,” *Phys. Rev. E* **93**, 032123 (2016).
- [51] T. Aspelmeier, Wenlong Wang, M. A. Moore, and Helmut G. Katzgraber, “Interface free-energy exponent in the one-dimensional Ising spin glass with long-range interactions in both the droplet and broken replica symmetry regions,” *Phys. Rev. E* **94**, 022116 (2016).
- [52] Miguel Aguilar-Janita, Silvio Franz, Victor Martin-Mayor, Javier Moreno-Gordo, Giorgio Parisi, Federico Ricci-Tersenghi, and Juan J. Ruiz-Lorenzo, “Small field chaos in spin glasses: Universal predictions from the ultrametric tree and comparison with numerical simulations,” *Proceedings of the National Academy of Sciences* **121**, e2404973121 (2024).
- [53] Markus Manssen, Alexander K. Hartmann, and A. P. Young, “Nonequilibrium evolution of window overlaps in spin glasses,” *Phys. Rev. B* **91**, 104430 (2015).
- [54] A. Crisanti and C. De Dominicis, “Low-temperature mass spectrum in the Ising spin glass,” *Europhysics Letters* **92**, 17003 (2010).
- [55] A Crisanti and C De Dominicis, “Stability of the Parisi solution for the Sherrington–Kirkpatrick model near  $T = 0$ ,” *Journal of Physics A: Mathematical and Theoretical* **44**, 115006 (2011).
- [56] M. A. Moore, Hemant Bokil, and Barbara Drossel, “Evidence for the Droplet Picture of Spin Glasses,” *Phys. Rev. Lett.* **81**, 4252–4255 (1998).
- [57] C Rulquin, P Urbani, G Biroli, G Tarjus, and M Tarzia, “Nonperturbative fluctuations and metastability in a simple model: from observables to microscopic theory and back,” *Journal of Statistical Mechanics: Theory and Experiment* **2016**, 023209 (2016).
- [58] A. B. Harris, T. C. Lubensky, and Jing-Huei Chen, “Critical Properties of Spin-Glasses,” *Phys. Rev. Lett.* **36**, 415–418 (1976).
- [59] Jing-Huei Chen and T. C. Lubensky, “Mean field and  $\epsilon$ -expansion study of spin glasses,” *Phys. Rev. B* **16**, 2106–2114 (1977).
- [60] Maria Chiara Angelini and Giulio Biroli, “Real Space Migdal – Kadanoff Renormalisation of Glassy Systems: Recent Results and a Critical Assessment,” *Journal of Statistical Physics* **167**, 476–498 (2017).
- [61] Naomichi Hatano and J. E. Gubernatis, “Evidence for the double degeneracy of the ground state in the three-dimensional  $\pm J$  spin glass,” *Phys. Rev. B* **66**, 054437 (2002).